Advances in Water Resources

Advances in Water Resources 31 (2008) 561–576

Turbulence characteristics of flow region over a series of 2-D dune shaped structures

Satya P. Ojha, B.S. Mazumder *

Fluvial Mechanics Laboratory, Physics and Earth Sciences Division, Indian Statistical Institute, Calcutta 700 108, India

Received 27 February 2007; received in revised form 30 November 2007; accepted 4 December 2007
Available online 14 December 2007

Abstract

This paper addresses the development of a flow region associated with turbulence and stress characteristics over a series of 2-D asymmetric dunes placed successively at the flume surface. Experiments were conducted over twelve asymmetric dunes of mean length 32 cm, crest height 3 cm and the dune width almost as wide as width of the flume, using 3-D Micro-ADV at the Indian Statistical Institute, Calcutta. The variations of turbulence statistics along the flow affected by the wavy bottom roughness have been studied. Quadrant decomposition of the instantaneous Reynolds shear stress has been adopted to calculate the contribution of ejection and sweeping events in shear stress generation. The relative dominance of two events are found to contribute in a cyclic manner (spatially) in the near bed region, whereas such phenomenon seems to be disappeared towards the main flow.

Keywords: Turbulent boundary layer; Dunes; Flow separation; Reynolds stress; ADV; Conditional statistics

1. Introduction

Dunes are the most common bed form structures in sandy rivers. Knowledge of the turbulence characteristics of the complex flow regimes found over typical bed forms or dunes must be known to predict the behavior of many natural phenomena. Dunes in bed load-dominated and/or laboratory environments are often asymmetric having low-sloping upstream side (stoss) and steep lee faces [12,17], while those in suspended load dominated environments are often more symmetric with relatively low angle lee faces [19,3]. The bed forms, such as ripples and dunes, play an important role in controlling sediment transport rates, generating turbulence and creating flow resistance, so it is essential that a detailed understanding be acquired of turbulence characteristics over two dimensional dunes. Experimental and field investigations of dunes have documented the macro-turbulent characteristics of spatially varied flow over the bed forms called "kolks" and "boils" proposed by Matthes [25]. The "kolks" and "boils" are the upward tilting vortices of both fluid and sediment originated from downstream of dune crests and at the point of reattachment. On the basis of the observation on "kolks" proposed by Matthes, Sengupta [36] suggested that such action in the stream bed might be responsible for initiation of trough type cross-beddings in river beds. Several experiments were performed to estimate the resistance to the flow due to the physical changes of bed forms generated by the turbulent flow [34,10]; and others. Wiberg and Nelson [41] conducted the laboratory experiments under unidirectional flow over asymmetric and symmetric features including high-angle and low-angle ripples. Lyn [21] reported the experimental study on the mean flow and turbulence characteristics over artificial space-periodic one-dimensional bed form features using 2-D laser Doppler velocimetry (LDV). Bennett and Best [1] suggested that the bursting events due to turbulent flow are associated with the zone of Kelvin–Helmholtz instabilities developed at the zone of flow separation in front of ripple lee. Venditti and Bennett [40] used the spectral and co-spectral analysis

to describe the characteristics of turbulent flow and suspended sediment transport over fixed dunes. Best et al. [2] performed a field study at the Fraser River Estuary, Canada followed by the experimental study in the laboratory using ADVP to provide detailed quantitative visualisation of flow fields associated with natural sand dunes. The structure of mean flow and turbulence over the fixed, artificial, asymmetric, three-dimensional dunes in laboratory channel has been studied by Maddux et al. [22,23]. Best [4] has made an excellent review to summarize the features of mean flow, turbulence, morphology and sediment transport associated with the river dunes and highlighted the future directions of research to understand the dynamics of dunes. The motivation of this study was to determine the spatial changes of flow and turbulence over bed forms, and to gain better understanding of the physics of flow, which are responsible for sediment size sorting and transportation.

In spite of the considerable work mentioned above, little attention has been paid to the development of rough-bottom turbulent boundary layer thickness associated with the turbulence statistics of flow over a series of asymmetric dunes placed consecutively at equal distance. In order to achieve a general output regarding the turbulence accumulating along the flow over series of dunes, it is desirable to analyse the physics of turbulence from the velocity data collected using ADV at different stream-wise locations. Therefore, the present study addresses how the turbulence characteristics of flow vary along a series of static dunes. It also elucidates how the conditional shear stress statistics characterizes the reattachment points in the flow over a trough region. The deviations of velocity, turbulence and the fractional contributions of burst-sweep cycles to the total shear stress due to the presence of dune covered topography would require substantial investigations. The approximation of 2-D static dune configuration is justified because the speed of the sand dunes is small compared with the mean flow. Moreover, the use of fixed bedforms allows a high spatial resolution of analysis and sampling very close to the boundary which is not possible with mobile bedforms. The mobility of the bedforms governs the turbulence near the boundary and hence the transition of the bedforms. In the field, reliable velocity measurements in the lee side of the dune is very difficult. The contamination in data or loss of data leads to overestimation of spatially averaged velocity over the dunes and hence the overestimation of shear stress in this region [18]. Robert and Uhlman [35] performed an experimental study to understand the processes of ripple-dune transition in the laboratory. In order to avoid the difficulty of velocity measurement during the ripple-dune transition they moulded three kinds of bedform features created under mobile flow conditions and performed experiments by fixing those moulded structures in the laboratory. Although the fixed bedform is not a correct representation of the natural dunes, the study over fixed dunes will improve the understanding of turbulence over dunes. The use of fixed bedforms allows the detail study of flow without added difficulty of measurement over mobile bed. Smith and McLean [37] reported from the field that in bed load dominated environment sand waves are relatively steep and very asymmetric, while in the suspended load dominated case they are more elongated and more symmetrical. The fixed dunes in the present study can be assumed to mimic the equilibrium dunes found in the bed load dominated environment. As the bed forms observed in the flume studies involve complex geometry, a train of asymmetric dunes have been chosen to elucidate the essential mechanism of the flow and circulation patterns over the waveform structures. This study addresses the spatial changes of flow characteristics and turbulent events associated with the burst-sweep cycle over the train of waveforms. It aims at improving the understanding of the phenomena which are crucial for the process of sediment transport, upliftment and grain-sorting.

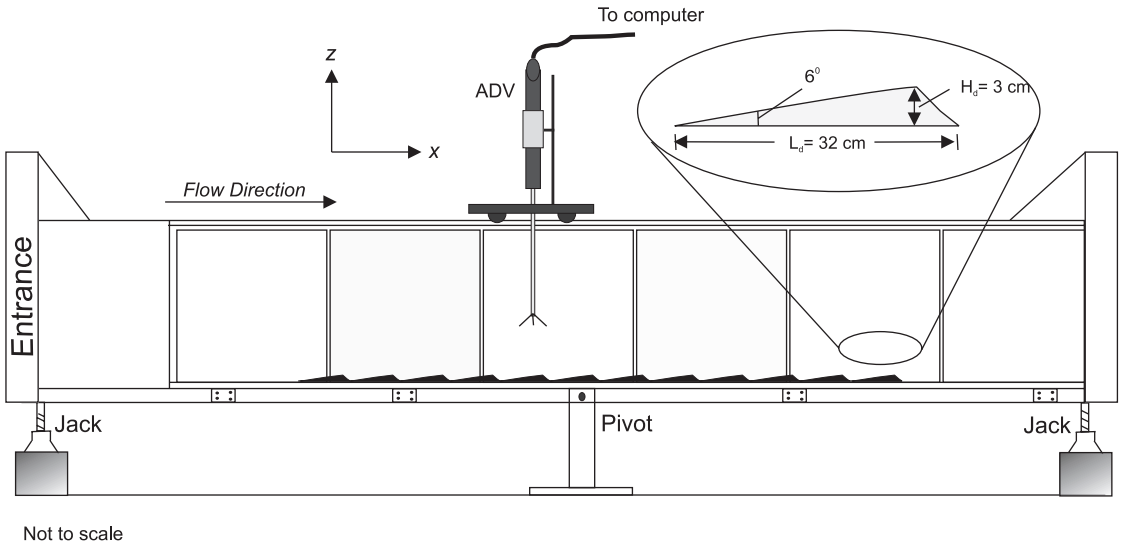

Fig. 1. Schematic diagram of the experimental setup.

2. Experimental details

The experiments were carried out in a specially designed re-circulating flume (Fig. 1) at the Fluvial Mechanics Laboratory, Physics and Earth Sciences Division, Indian Statistical Institute, Kolkata [26,27]. Both experimental and re-circulating channels of the flume are of the same dimensions (10 m long, 0.5 m wide and 0.5 m deep). The experimental walls of the flume are made of perspex windows with a length of 8 m, providing a clear view of the flow. One centrifugal pump providing the flow is located outside the main body of the flume. The inlet and outlet pipes are freely suspended from the overhead structure to allow tilting of the flume. The outlet pipe is fitted with one by-pass pipe and a valve, so that by adjusting the valve in the outlet, the flow can be controlled at a desired speed. Two honeycomb cages are placed in front of the outlet pipe to ensure the smooth, vortex free, uniform flow of water through the experimental channel. An electromagnetic discharge meter with a digital display is fitted with the outlet pipe to facilitate the continuous monitoring of the discharge. To ensure the same operating conditions in different experiments the water depth and the discharge are kept constant for all experiments.

To perform the experiments, a total of twelve artificial 2-D dunes of synthetic plastic were fabricated and placed consecutively with equal distances on the bottom surface of the flume. Fig. 1 shows a schematic view of the experimental setup with acoustic Doppler velocimeter (ADV) for velocity measurements and a magnified picture of a dune. Joints between adjacent dunes were sealed with waterproof adhesive and the joints were made smooth. The dunes had mean wavelength, $\lambda_d = 32$ cm and mean height $H_d = 3$ cm at the crest which results in the steepness, $\frac{H_d}{\lambda_d} = 0.094$ which is consistent with values of $\frac{H_d}{\lambda_d}$ for real dunes in field [11,16]. The angles of the stoss side and lee side slope of the dunes were approximately 6° and 50°, respectively (see Table 1). Each dune spanned almost the width of the flume. Dunes were painted with epoxy paint to make the surface smooth. The counting of the dunes starts from the very first dune at the upstream end, which is about 3.3 m away from the beginning of the channel inlet. All together twenty six different measuring locations at the trough and crest points of the dunes starting from the very first dune of the series from upstream to downstream have been selected. In order to find the uniform flow region along the flow and to determine the rough-bottom turbulent boundary layer development, velocity and turbulence profiles are measured by means of SonTek 16 MHz 5 cm down-looking 3-D-Micro ADV at the centerline of the channel. 3-D-Micro ADV is high precision instrument that measures all three components of velocity with fluctuations. The flow is measured from 5 cm below the probe and is practically undisturbed by the probe. Factory calibration of the ADV is specified to be ±1.0% [38]. The ADV has been validated with several other devices by several investigators and has been used in a variety of applications for turbulence measurements. The velocity data were collected for five minutes at the sampling rate of 40 Hz with the lowest point in each profile being 0.40 cm above the flume bed surface and with the highest point being about 24 cm for each profile.

Table 1
Hydrodynamic parameters and bed conditions

Plane bed	
Reynolds number, $Re = \frac{u_m h}{\nu}$	1.5×10^5
Maximum flow velocity, u_m (cm/sec)	50
Mean flow depth, h (cm)	30
Froude number, Fr	0.29
Friction velocity (from log law), u_* (cm/sec)	2.474
Nikuradse roughness, k_s (cm)	0.25
Dune covered bed	
Dune height, H_d (cm)	3
Dune width, W_d(cm)	50
Dune length, λ_d (cm)	32
Dune height-to-length ratio, $\frac{H_d}{\lambda_d}$	0.094
Lee side angle, (in degrees)	50
Stoss side angle, (in degrees)	6
Mean flow velocity, (depth average) $\bar{u_d}$ (cm/sec)	30
Dune height-to-depth ratio, $\frac{H_d}{h}$	0.1
Friction velocity (from Eq. (7)), u_{*w} (cm/sec)	4.00
Modified Nikuradse roughness, k_{sw} (cm)	5.65

The mean flow depth h is kept constant at 30 cm for all tests. For each experiment, the velocities were measured at the centerline at about 35 vertical positions. Here, the experiments were performed at a discharge $Q = 0.04$ cubic m/sec. In fully developed turbulent flow on the flat surface the Reynolds number was found to be $Re = \frac{u_m h}{\nu} = 1.50 \times 10^5$; and the Froude number, $Fr = \frac{u_m}{\sqrt{gh}} = 0.29$, where u_m (=50 cm/s) is the maximum velocity observed at the height $z = 24$ cm above the flat surface, ν is the kinematic viscosity of water, and g is acceleration due to gravity. While doing experiments over the dune covered bed the flow conditions (Table 1) are kept same as on the flat surface.

3. Experimental results

The velocity data collected by ADV are analyzed to compute the mean flow and turbulence characteristics at each point. The time averaged stream-wise velocity $\bar{u}$, vertical mean velocity $\bar{w}$, stream-wise turbulence intensity $\sqrt{\overline{u'^2}}$ and vertical turbulence intensity $\sqrt{\overline{w'^2}}$ are defined as

$$\bar{u} = \frac{1}{n}\sum_{i=1}^{n} u_i, \tag{1}$$

$$\bar{w} = \frac{1}{n}\sum_{i=1}^{n} w_i, \tag{2}$$

$$\sqrt{\overline{u'^2}} = \sqrt{\frac{1}{n}\sum_{i=1}^{n}(u_i - \bar{u})^2}, \tag{3}$$

$$\sqrt{\overline{w'^2}} = \sqrt{\frac{1}{n}\sum_{i=1}^{n}(w_i - \bar{w})^2}, \tag{4}$$

where n is the total number of velocity observations at each point. The time averaged local Reynolds shear stress at a point is determined using

$$\tau = -\rho\overline{u'w'}, \tag{5}$$

with

$$\overline{u'w'} = \frac{1}{n}\sum_{i=1}^{n}(u_i - \bar{u})(w_i - \bar{w}), \tag{6}$$

where the prime denotes fluctuations of velocity and ρ is the fluid density. To ensure the fully developed flow at the sampling station we performed three experiments at three different locations in the downstream direction and found almost no change amongst the results of those tests. The results of all three experiments on flat surface are plotted together in Fig. 2. Fig. 2a–c shows the normalized mean velocity, turbulence intensity and the Reynolds shear stress profiles over the flat bed surface. Here the parameters are normalized by the friction velocity u_* obtained from the log-law and plotted against the non-dimensional distance z/h. The results on the plane bed surface are in good agreement with previous work [31].

3.1. Mean velocity profiles

The vertical profiles of mean velocity components ($\bar{u}$, $\bar{w}$) at the trough and crest points along the stream-wise direction illustrate the characteristic features of turbulent flow. Fig. 3a and b shows stream-wise mean velocity profiles at the trough and crest points, respectively, of each dune. In the figures, odd numbers inside circles represent the positions of velocity profiles in the consecutive trough points starting with 1 at the tail point of the first dune and even numbers inside circles represent the positions of the velocity profiles at the crest point starting with 2 at the first dune crest. In order to highlight the relative changes of turbulence parameters, a comparative study has been made between the velocity profiles at the flat surface and that observed at the trough and crest positions. Two loci of the points of intersections between the velocity profiles on the flat surface and the dune covered bed are drawn, which lead to focus the flow evolution over the dune covered bed (Fig. 3a and b). The line clearly shows the developing flow from the leading dune up to the seventh dune and then it reaches to quasi steady state. It appears from the Fig. 3a that the existence of flow separation, flow reversal and sudden expansion significantly occurs. Three distinct layers are observed: (1) internal layer, $z/h \leqslant 0.05$; (2) the advecting and diffusing region, $0.05 \leqslant z/h \leqslant 0.15$; and (3) the outer flow region, $z/h \geqslant 0.15$. For a better view of the flow region at the trough positions near the bed a close up view (near bed) of the Fig. 3a is given in Fig. 3c. The stream-wise mean velocity profiles at the trough positions have inflexion points near the bottom resulting in flow instability in the near bed region. The velocity in the

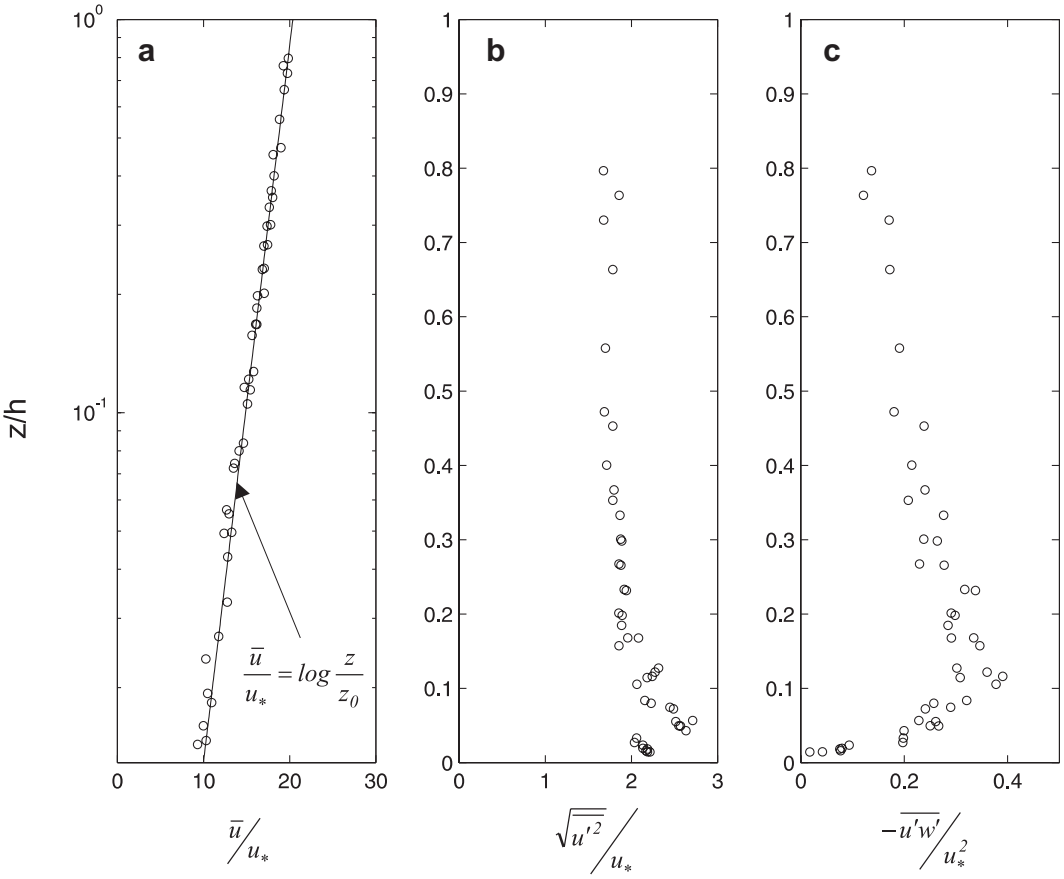

Fig. 2. Plots of normalized mean velocity, turbulence intensity, and Reynolds shear stress on the plane rigid surface.

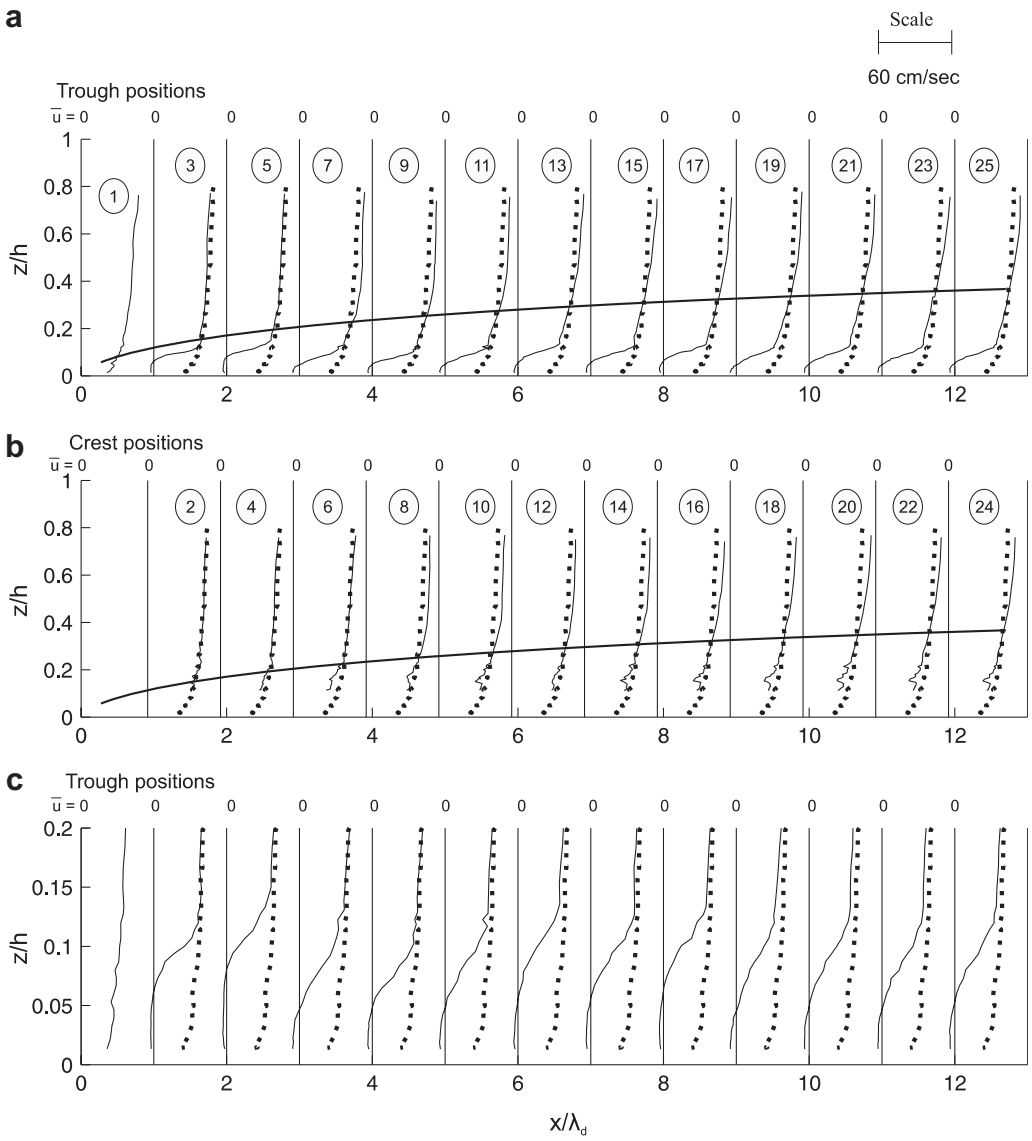

Fig. 3. Stream-wise mean velocity $\bar{u}$ over dune covered surface: (a) at the trough positions, (b) at the crest positions and (c) near bed profiles at the trough positions. Dotted profile represents for the plane surface. 1 (in circle) represents the vertical profile at the beginning of the first dune. Odd numbers (in circle) indicate the vertical profiles at the trough positions and the even numbers for the crest positions. Vertical lines (zero line) in (a) are placed at the trough positions and in (b) are placed at the crest positions. The solid curved lines (growth curve) are drawn by joining the points of intersection of profiles at dune covered surface and the profiles at the plane surface.

upper region of the flow seems to be larger than that at the flat surface except for the first two dunes. The region of larger velocities decreases downstream indicating the development of the turbulent boundary layer due to the dune covered bed. The positions of the collapsing points in the individual profiles, representing a locus, show that the turbulent boundary layer grows over the dune covered bed. Some scattering of the data is observed at height $0.1 \leqslant z/h \leqslant 0.2$ in the stream-wise mean velocity profiles at the crest locations (Fig. 3b) which may be attributed due to the flow separation. It is observed that at the crest level the horizontal velocity at the crest and the trough locations is smaller than that on the plane surface at that level. The reason of reduced stream-wise velocity at crest is given later.

The profiles of the time-averaged vertical velocity component ($\bar{w}$) at different stream-wise distances (x/λ_d) are plotted in Fig. 4a for trough positions and in Fig. 4b for crest positions. At the trough positions, it is observed that the velocity profiles ($\bar{w}$) first increases up to the level $z/h \leqslant 0.05$, then decreases, crossing the zero velocity within the region $0.05 \leqslant z/h \leqslant 0.1$ which is below the crest level. This implies that the streamlines are first directed upward and then directed downward towards the bed. Above the crest level the mean velocity shows some irregular behavior up to the seventh dune (No. 15, $x/\lambda_d = 7$), where the veloc-

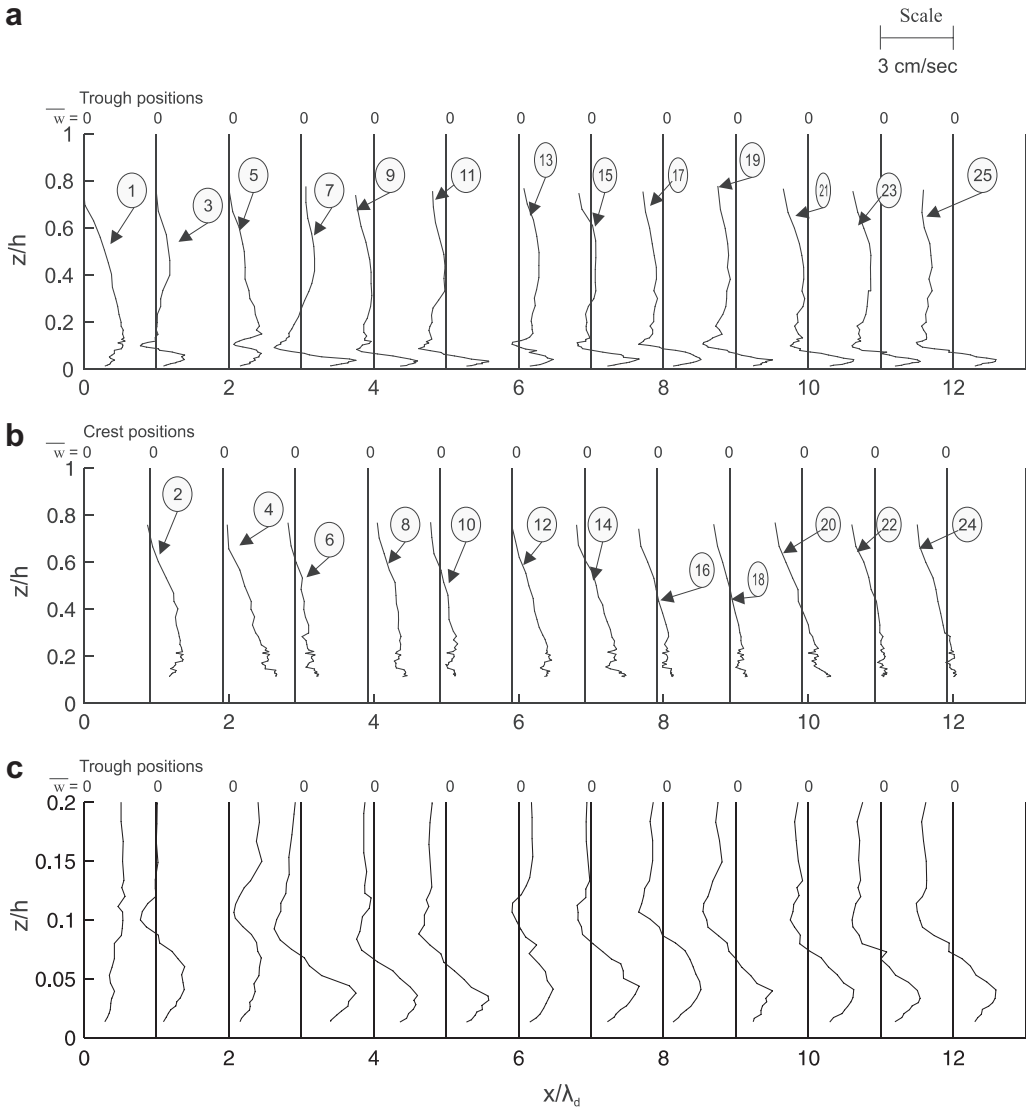

Fig. 4. Vertical mean velocity over the dune covered bed: (a) at the trough positions, (b) at the crest positions and (c) near bed profiles at the trough positions. Numbers in circle indicate as in Fig. 3.

ity ($\bar{w}$) is almost zero through out the depth; then it becomes stable with a downward velocity through out the depth. Fig. 4b shows that at the crest position the direction of $\bar{w}$ changes from upward to downward at the outer part of the flow domain. Along the downstream direction the position of the zero velocity point shifts toward the crest, barring eleventh dune crest profile (No. 22), and forms a locus above which the downward directed velocity gets much more significant than the upward velocity below the locus. Close up view of the near bed vertical velocity profile at the trough positions is given in Fig. 4c.

Fig. 5a shows the vector plot of the flow field over a complete trough region between two consecutive dunes (9th and 10th) in the fully developed roughness turbulent boundary layer indicating the circulation region at the lee side of the dune. Flow is directed upward over the stoss side of the dune and downward past the crest into the trough. The occurrence of greatest upward velocity at the crest is likely to be responsible for the reduction of stream-wise flow over the crest (Fig. 3b). Just after the crest position strong downward flow occurs which leads to decrease the stream-wise velocity (Fig. 3a). The center of the circulation bubble appears to be located at a distance of about $2.67H_d$ downstream and $0.75H_d$ below the point of separation. The distance between the point of separation and the point of reattachment is about $5.8H_d$ which agrees well with Engel [9]. The streamlines are also shown in Fig. 5a. Convex streamline curvature serves to stabilize vertical components of turbulence and concave curvature destabilizes flow by conveying turbulent structures toward the surface [5]. The streamline at the crest level changes its curvature from convex to concave. This inflexion in the streamline indicates that the flow separation occurs twice [24]: one at the crest and other one at a distance about H_d downstream from the crest. Two separation points are marked as circles in Fig. 5a. The close up views of vector plots given in

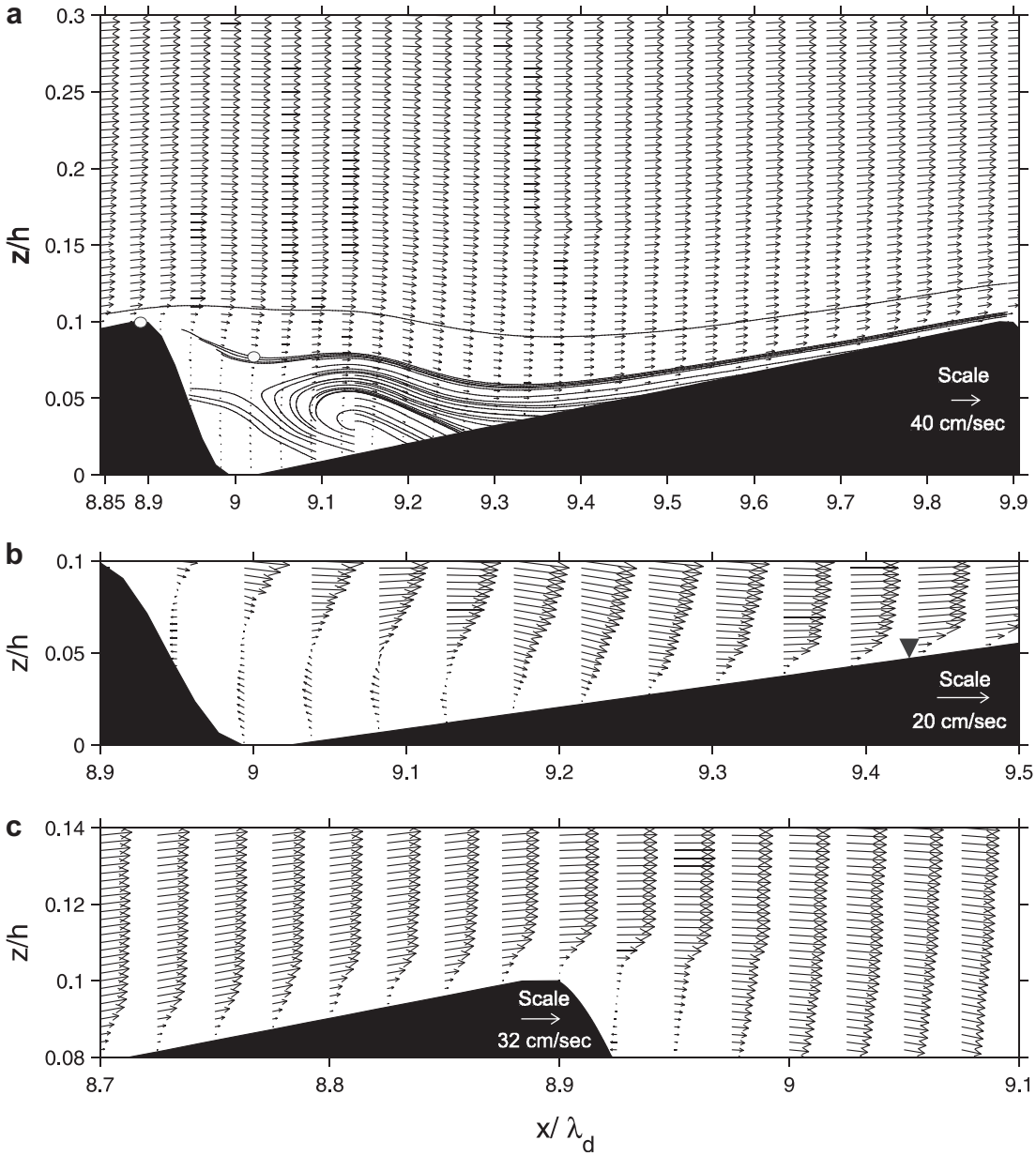

Fig. 5. (a) Velocity vector plot between 9th and 10th dune in the fully developed region. Two circles represent the points of separation. Solid lines represent the streamlines of the flow. (b) Close up view (near trough region) of (a). (c) Close up view of the vector plot over the crest position.

Fig. 5b and c provide clear picture of the flow phenomena at the trough and crest positions, respectively.

3.2. Friction velocity and roughness due to dune covered bed

In order to determine a zero-order velocity profile to use in perturbation theories for non-uniform flows of finite depth the actual velocity field can be spatially averaged over one wavelength along lines of constant distance from the bottom surface. The term 'spatially averaged' in the velocity field is used to reduce substantially the errors due to the non-uniformity of flow over the wavelength. This approach assigns all the important nonlinear effects due to second and higher order terms to the zero-order profile and provides a mechanism whereby the zero-order velocity profiles can be constructed for two dimensional channel flows [37]. Averaging the velocity data along the lines of constant distance from the bottom surface over the wavelength, the law of wall for flow field in its general form [32] with zero-plane displacement z_d can be written as:

$$\frac{\langle \bar{u} \rangle}{u_{*w}} = \frac{1}{\kappa} \ln \frac{z - z_d}{z_0}, \tag{7}$$

where $\langle \bar{u} \rangle$ is the spatially averaged velocity, $\kappa (= 0.4)$ is the von-Karman constant, z_0 is equivalent bed roughness and u_{*w} is the friction velocity due to bottom waves. Using the measured velocity $\langle \bar{u} \rangle$, $\kappa = 0.4$, the values of the modified shear velocity u_{*w}, the modified roughness parameter

k_{sw}, and zero-plane displacement z_d can be determined from Eq. (7). This technique enables the determination of z_d directly from the spatially averaged velocity profile without prior knowledge of the shear velocity. The value of z_d which gives the best fit of the spatially averaged velocity data with the velocity profile (7) should be taken as zero-plane displacement thickness.

In order to determine the zero-order velocity profile in this study, spatial-averaging is performed at each distance above the plane surface over eleven vertical velocity profiles for a dune length. Following the above mentioned procedure the values of z_d and k_{sw} are found to be 1.50 cm and 5.65 cm, respectively. In literature, different relations between the bed roughness k_{sw} and the ripple characteristics may be found. In general, the modified bed roughness due to dune-covered surface k_{sw} is assumed to be proportional to the product of ripple height H_d and ripple steepness $\frac{H_d}{\lambda_d}$, that is,

$$k_{sw} = C_d H_d \frac{H_d}{\lambda_d}, \tag{8}$$

where C_d is a constant whose value varies between 9 and 90 [39]. The plot of the spatially averaged stream-wise velocity profile over one dune length is shown in Fig. 6 along with the logarithmic fit. The log law is valid up to 10 cm only. The definition of the origin of the z-axis ($z = 0$) with respect to the dune geometry affects the resulting value of z_0 and hence value of k_{sw}. Therefore, the position of the origin of the z-axis has to be taken into consideration to compare reported values of k_{sw}. The value of the modified friction velocity u_{*w} is obtained as 4.00 cm/sec due to dune-covered surface (see Table 1).

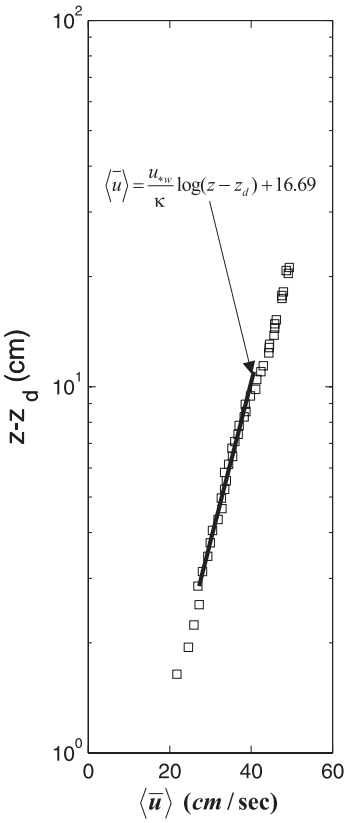

Fig. 6. Spatially averaged stream-wise mean velocity profile over one dune length in the fully developed region.

3.3. Turbulence intensities and shear stress

The vertical profiles of stream-wise turbulence intensity component $\sqrt{\overline{u'^2}}$ at different x/λ_d along the downstream direction are plotted in Fig. 7a for the trough and in Fig. 7b for the crest locations together with the turbulence intensity observed at the plane surface. A close view of the near bed turbulence intensity profile at the trough positions is also shown in Fig. 7c. Two lines joining the intersecting points of the turbulence intensities from the flat plate and the dunes, respectively, are drawn in the downstream direction for the trough and crest locations. It is observed from the figures that the shifting of intersecting points towards the outer flow from trough to trough and crest to crest leads to an increase in the turbulence intensity in the upward direction (free turbulent area) as the form roughness turbulent boundary layer increases. The rate of increase goes up to seventh dune from the leading dune and then reaches a quasi-steady state at the level $z/h = 0.7$. It also reveals that the stream-wise turbulence intensity profiles at the trough locations first increases with height near the bed with maximum at $z/h = 0.1$ and then decreases with minimum up to the level $z/h \leqslant 0.2$. This boundary-layer like behavior of the turbulence intensity may be because of the form roughness boundary layer formation at the dune covered surface. The vertical component of the turbulence intensity $\sqrt{\overline{w'^2}}$ along x/λ_d over each trough and crest are presented in Fig. 8a and b together with the corresponding intensity measured at the plane surface. The close up view of the near bed vertical turbulence intensity at the trough positions is also shown in Fig. 8c. It is observed that the position of the intersecting points is shifted upwards in the downstream direction. Thus, it is interesting to notice that the rate of increase of turbulence intensity gradually increases along the flow due to the accumulation of turbulence generated from the series of dunes, which clearly shows the deviations of the turbulence intensities from the reference intensity at the plane surface. Furthermore, due to the separation of flow at the crest level, two peaks are noticed at the trough positions: one at the crest level height and other one in the free turbulent area above the crest level where the shear mixing layer presents. The peak above the crest level could be the remnant/residual of the previous dune.

Fig. 9a and b displays the vertical profiles of Reynolds shear stress ($-\rho\overline{u'w'}$) against x/λ_d over each trough and crest positions together with the corresponding shear stress profiles observed for the plane surface as reference. Near bed variation of the shear stress at the trough positions is shown in Fig. 9c. It is observed that the shear stress increases upwards with downstream distance from the first

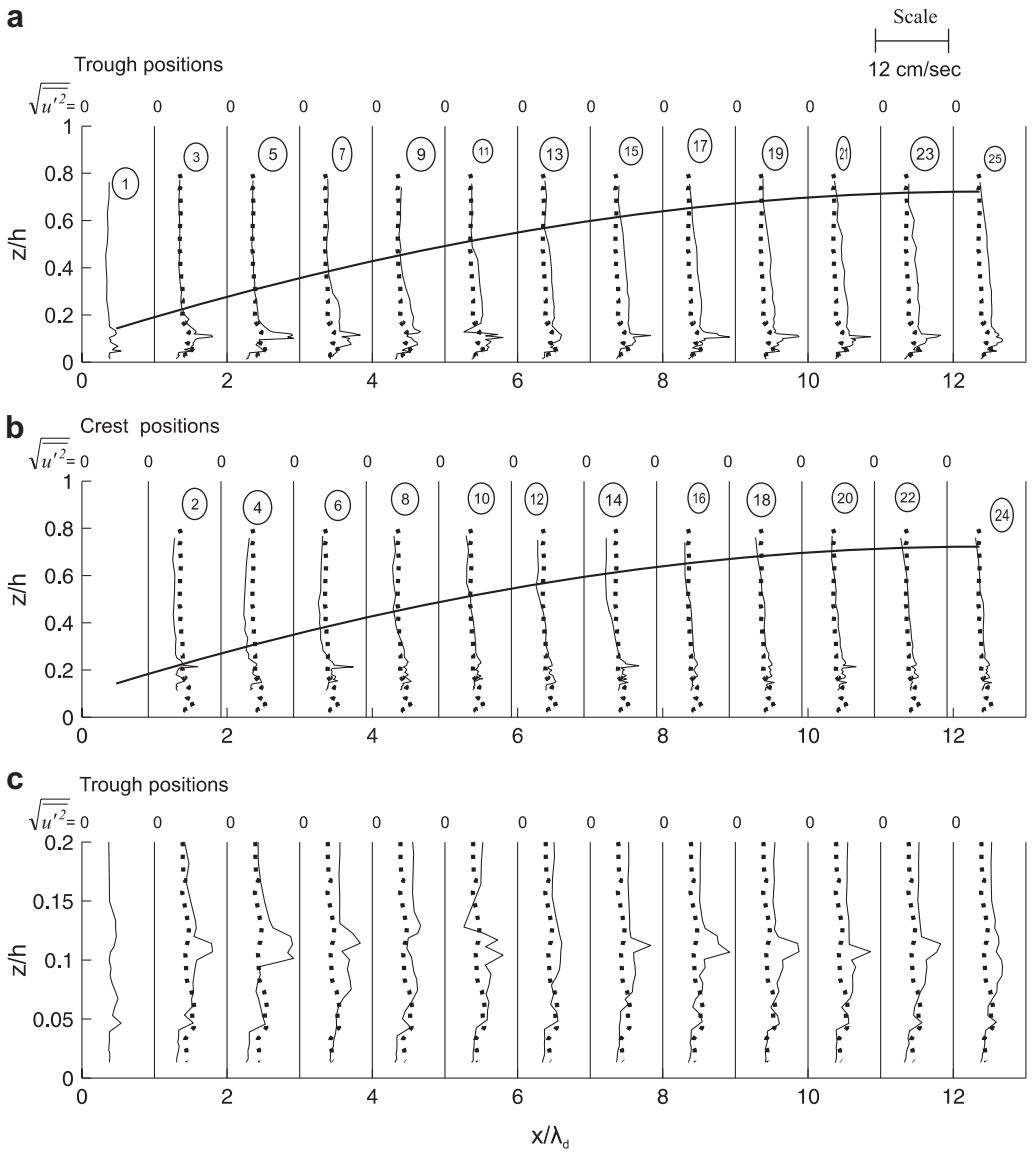

Fig. 7. Stream-wise turbulence intensity $\sqrt{\overline{u'^2}}$ over the dune covered surface: (a) at the trough positions, (b) at the crest positions and (c) near bed profiles at the trough positions. Dotted profiles represent the turbulence intensity over the plane surface. Captions as in Fig. 3.

dune. At the trough position the shear stress profiles exhibit two peaks- one at the crest level $z/h = 0.1$ and other one above the crest at $z/h = 0.2$, that is, the larger maximum stresses are located along the shear layer above the crest level [1,22]. The peak above the crest level could be the remnant of the upstream dune, riding above the new ones created on the current dune. Observation reveals that shear stress increases significantly both at the trough and crest locations compared with that for the plane surface. The shear stresses increase upwards with the distance x/λ_d, representing higher turbulence. In the figures, the lines represent the vertical locations of minimum shear stresses along the flow and clearly show the growth of shear stress region (depth-wise). The growth of shear stress indicates that the downstream flow is not only capable of transporting more sediment near the bed (bed load), but it has also more potential to carry the sediment as suspended load. It is observed from the figures that the maximum shear stress attains at the separation point ($z/h = 0.1$) for the trough locations (Fig. 9a) and at the height $z/h = 0.2$ for the crest (Fig. 9b) where turbulence generated by the separated shear layer had the least distance be transported by advection or diffusion before interacting with the bed. The high magnitude of shear stresses near the bed could be responsible for the erosion of scour pits over the dunes [8,7]. It is interesting to note that unlike the velocity and turbulence intensity profiles that approach an equilibrium state with distance downstream, the shear stress profiles continue to vary throughout the twelve dune shapes. The shear stress distribution at the crest is almost the same as obtained at the trough above the crest level. The peak in the shear stress profiles at the dune crest indicates the development

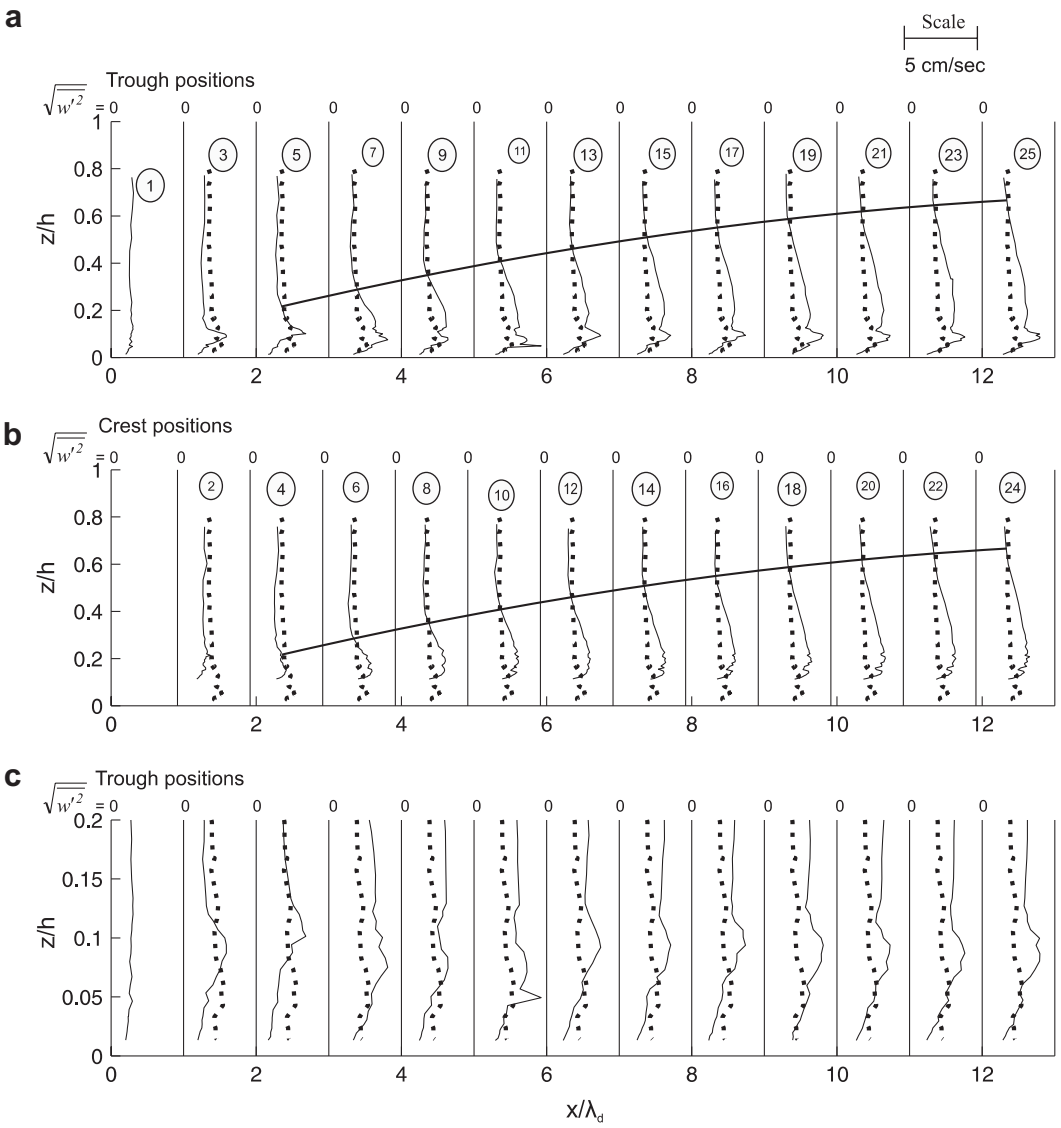

Fig. 8. Vertical turbulence intensity $\sqrt{\overline{w'^2}}$ over dune covered surface: (a) at the trough positions, (b) at the crest positions and (c) near bed profiles at the trough positions. Captions as in Fig. 3.

of local internal boundary layer (IBL) forming at the point of reattachment and extending up to the dune crest. This phenomenon is also visible from the vector plot (Fig. 5). Turbulence shear stress is found to increase in the outer region in the downstream direction at both crests and troughs. It appears from the figures that the thickness of 'effective shear stress layer' indicated by the locus of intersecting points increases till seventh dune ($x/\lambda_d \approx 7.0$) and the increment of this thickness is smaller and smaller along downstream, indicating the disappearance of entrance effects. So the region beyond the length $x/\lambda_d \approx 7.0$ can be considered effectively as fully developed region. The bottom shear stress ($\overline{\tau}_0 = -\rho\overline{u'w'}|_{\text{at dune surface}}$) at the dune surface elevation over two dunes (9th and 10th, $8 \leqslant x/\lambda_d \leqslant 10$) in the fully developed region is presented in Fig. 10. Values of bottom shear stress are estimated by extrapolating the Reynolds shear stress profiles down to the dune surface. Results show that bottom shear stress first increases and reaches a maximum value at the region of lower stoss side ($0.3\lambda_d$) and then decreases and reaches a minimum value at the dune crest. Ikeda and Matsuzaki [14] suggest that flow separation starts where the wall shear stress vanishes. Fig. 10 shows that the value of the boundary shear stress at the dune crest is almost zero. The over estimation of the boundary shear stress may be due to the error arising from the extrapolation down to the dune surface. Thus, Fig. 5b confirms the flow separation at the dune crest.

3.4. Conditional statistics of Reynolds shear stress

Coherent structures distribute particles and pollutants across the whole water column much faster than small-scale turbulence [13]. Cellino and Lemmin [6] demonstrated

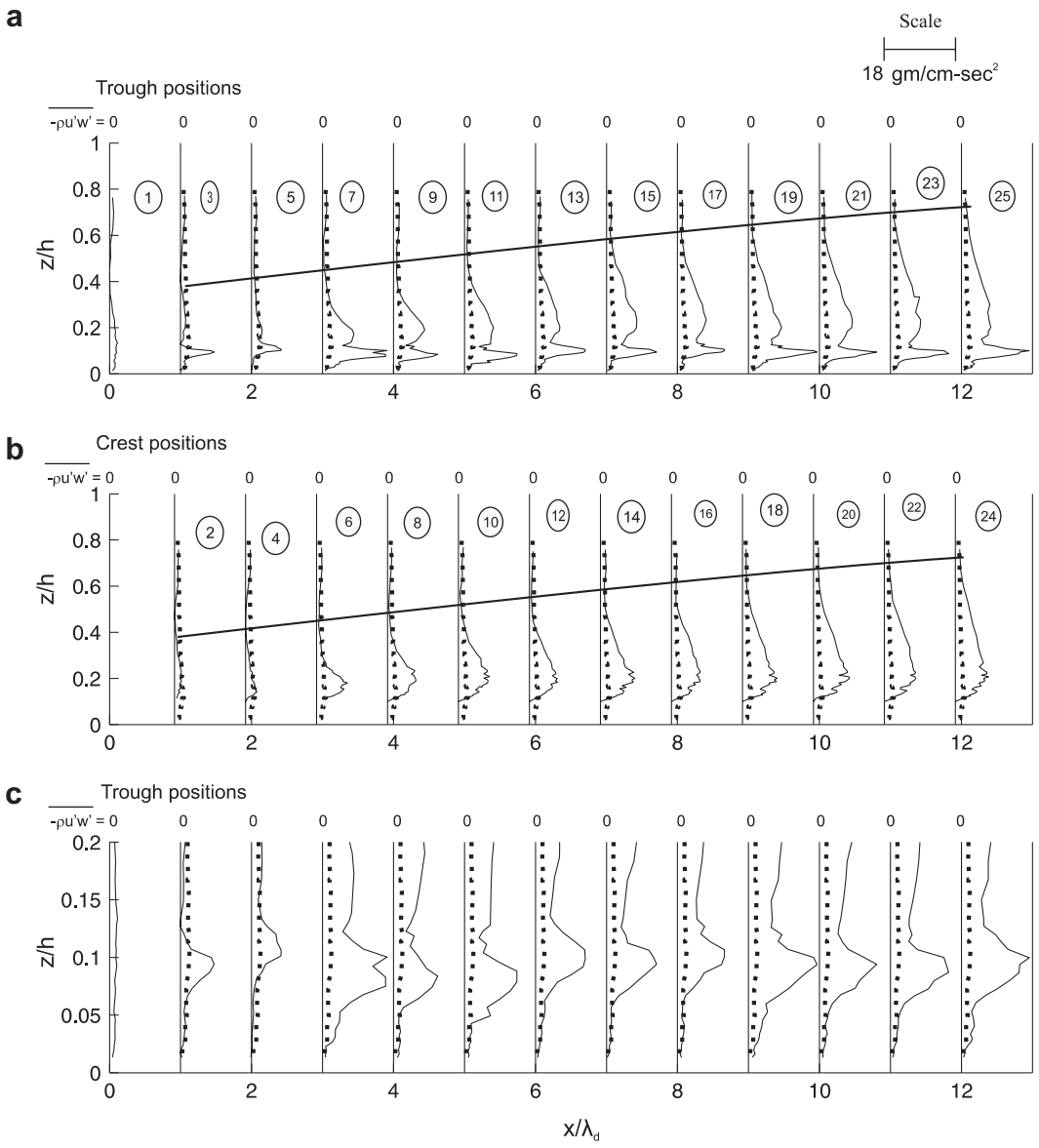

Fig. 9. Reynolds shear stress $-\overline{\rho u'w'}$ along the flow: (a) at the trough positions, (b) at the crest positions and (c) near bed profiles at the trough positions. Captions as in Fig. 3.

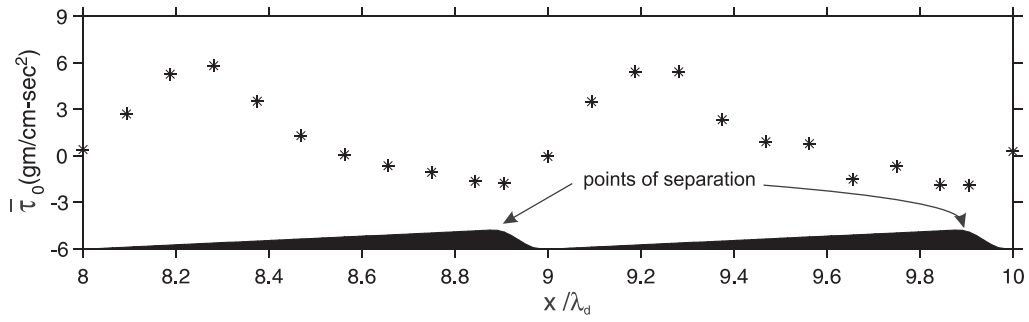

Fig. 10. Bottom shear stress distribution over two consecutive dune lengths (9th and 10th) in the fully developed region.

the importance of ejections and sweeps in sediment-laden flow. The study of 3-D instantaneous velocity fields in river flows is essential in order to understand the mixing and transport processes related to flow intermittency. Coherent structures have a short life span. They cannot be identified with a time averaged analysis. Therefore, it requires an

investigation based on time and space correlation measurements. In laminar and transitional flows, coherent structures occur periodically, whereas in turbulent flows they occur randomly in space and time. Hence, conditional sampling and statistics techniques have to be used in the detection and characterization of coherent structures. The conditional statistics technique may be applied to quasi-instantaneous velocity samples obtained from the ADV measurements. Several investigators applied conditional statistics to turbulence studies [20,28,33]. The turbulent events are defined by the four quadrants as outward interactions $(i = 1; u' > 0, w' > 0)$, ejections $(i = 2; u' < 0, w' > 0)$, inward interactions $(i = 3; u' < 0, w' < 0)$, and sweeps $(i = 4; u' > 0, w' < 0)$. At any point in a stationary flow, the contribution to the total Reynolds stress from quadrant i, excluding a hyperbolic hole region of size H, is

$$\langle u'w' \rangle_{i,H} = \lim_{T\to\infty} \frac{1}{T} \int_0^T u'(t)w'(t) I_{i,H} \mathrm{d}t, \tag{9}$$

where the angle brackets denote the conditional average and the indicator function $I_{i,H}$ obeys

$$I_{i,H}(u', w') = \begin{cases} 1 & if\,(u', w') \in i\text{th quadrant and } |u'w'| \geqslant H|\overline{u'w'}|, \\ 0 & \text{otherwise.} \end{cases}$$

Here H is the threshold parameter in the Reynolds stress signals, which enables us to extract those values of $u'w'$ from the whole set of data, which are greater than H times $|\overline{u'w'}|$ value. The stress fraction by ith quadrant defined above is

$$S_{i,H} = \frac{\langle u'w' \rangle_{i,H}}{|\overline{u'w'}|}, \tag{10}$$

and it satisfies

$$\sum_{i=1}^{4} |S_{i,H}| = 1. \tag{11}$$

We define

$$S_H = \frac{S_{2,H}}{S_{4,H}}, \tag{12}$$

which is a measure of relative dominance of sweeping and ejection events.

The above analysis is performed for all the experiments to study the relative dominance of four turbulent events described above. According to previous studies mentioned above the sweeping events are dominant in the near wall region of the flow, while ejections are dominant away from the boundary. Sweeping and ejections provide an extraction of energy from the mean flow field to generate turbu-

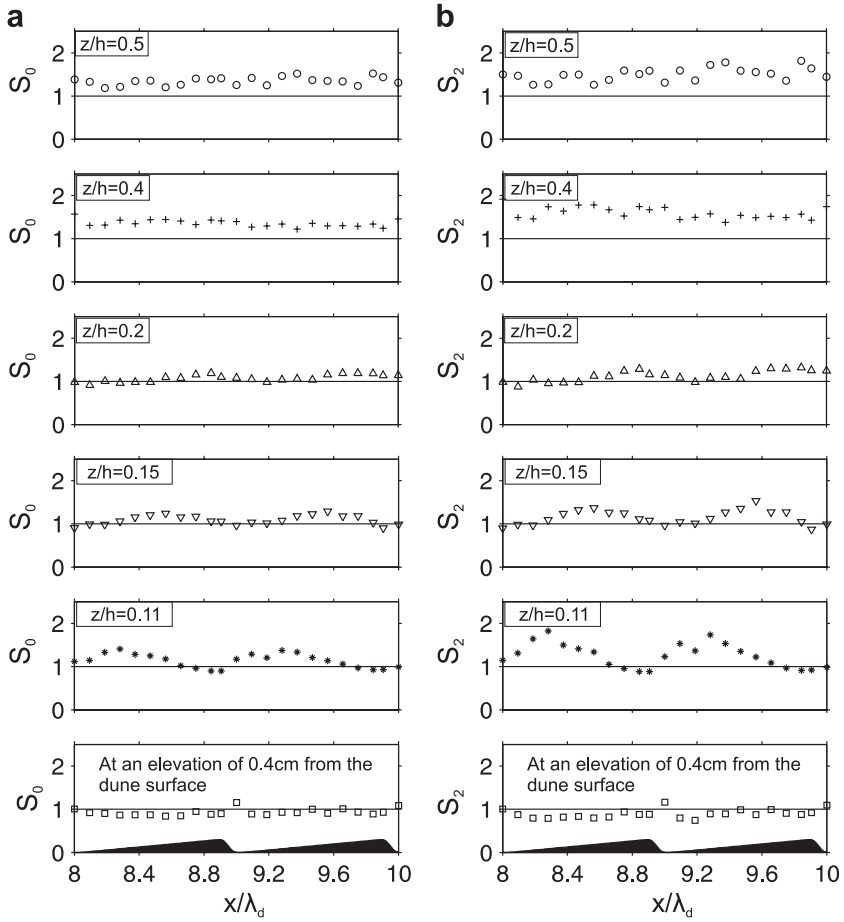

Fig. 11. Variation of S_H ($H = 0$, 2) over two dune lengths (9th and 10th) at five vertical heights and at 0.4 cm above the dune surface elevation.

lence, hence in sediment transport studies the sweep and ejection events are considered to be more important than the two interaction events. In order to predict the relative dominance of ejection and sweep events the ratios S_0 and S_2, computed at various heights ($z/h = 0.11, 0.15, 0.20, 0.40, 0.50$) over the 9th and 10th dune length ($8 \leqslant x/\lambda_d \leqslant 10$) together with the values computed at dune surface elevation, have been displayed in Fig. 11a and b. It is illustrated from the figures that S_0 and S_2 vary in an oscillatory pattern near the bottom, but at outer region $z/h = 0.4$ and 0.5 such pattern tends to be weak. It is interesting to note that at the dune surface the sweeping events are dominant throughout the dune length except at the trough location. Starting from the tail end of the dune, S_H $(H = 0, 2)$ decreases up to a length of about $0.6\lambda_d$ (where the reattachment point lies) and then increases to the trough point indicating the dominance of sweeping events in the separation region. At the level $z/h = 0.11$, for both values of H, sweeps are dominant only at the dune crests while ejections contribute more over the rest of the dune length. Moreover, the maximum value of S_0 and S_2 occurs at the stoss at a distance of about $0.3\lambda_d$ from the tail end of the dune. At $z/h = 0.15$ the sweep events contribute more than the ejection events only at the trough position; over the rest of the dune ejection events are dominant over the sweep events. The location of the maximum values of S_0 and S_2 is shifted downstream and is located at a distance of about $0.6\lambda_d$ from the tail end. Although the sweep events are not dominant anywhere at height $z/h = 0.2$, they are found to contribute equally with the ejection events at a distance of about $0.3\lambda_d$ from the tail of the dune. The maximum values of S_0 and S_2 occur just before the dune crest. At $z/h = 0.4$ and $z/h = 0.5$ ejection events are the dominant contributors over the whole dune length. In fact, this phenomenon is almost similar to that found on the flat surface [28,33], showing the negligible effect of bottom topographic features away from the boundary.

For a clear picture of the turbulent bursting events over the dune surface, the region of dominant quadrant events (Q2-Ejection, Q4-Sweeping) are shown in Fig. 12a–c for Q2 events (white color represents the ejection dominant region) and in Fig. 13a–c for Q4 events (white color represents the sweeping dominant region) for three values of H (=0, 2 and 4). The figures clearly show that the Q2 events make the dominant contribution to the shear stress in the lee side of the dune and in the outer region of the flow while Q4 events are dominant very near the dune surface. In the lee side of the dune it is noticed that the region of ejection

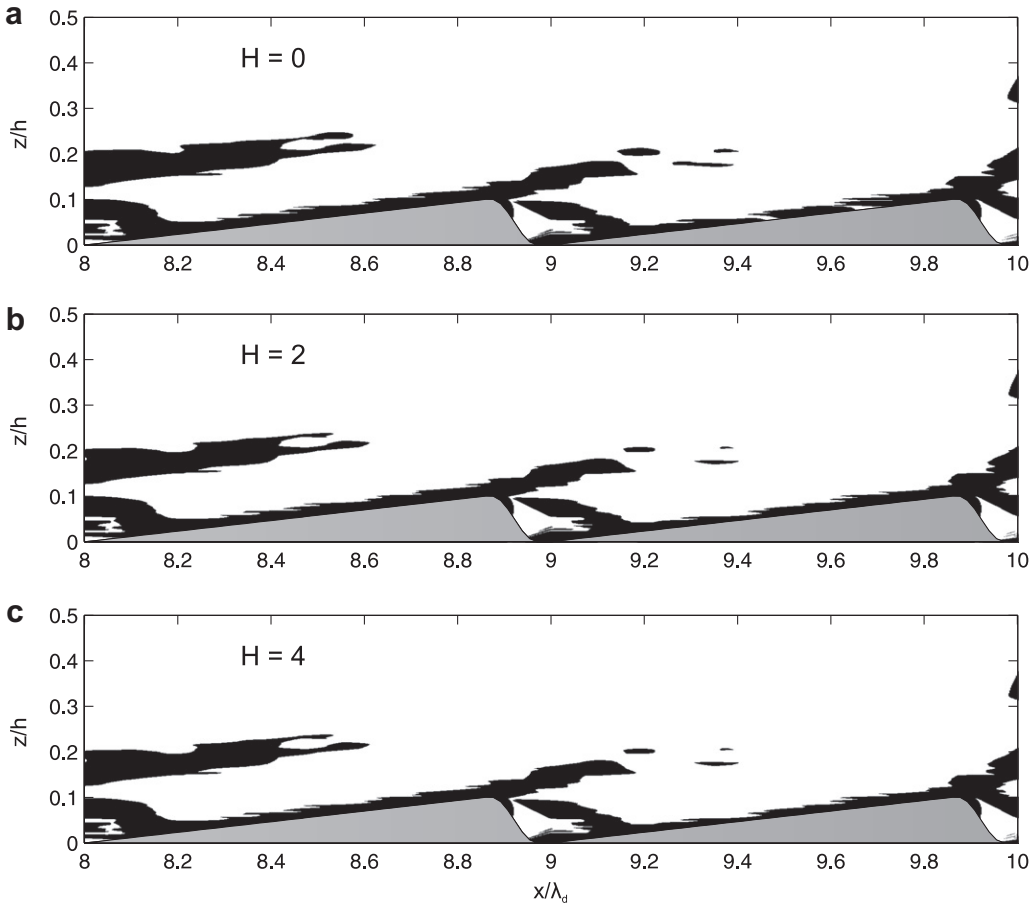

Fig. 12. Spatial distribution of the dominant ejection events: (a) for threshold parameter $H = 0$, (b) for $H = 2$, (c) for $H = 4$. White region represents the region of ejection dominance.

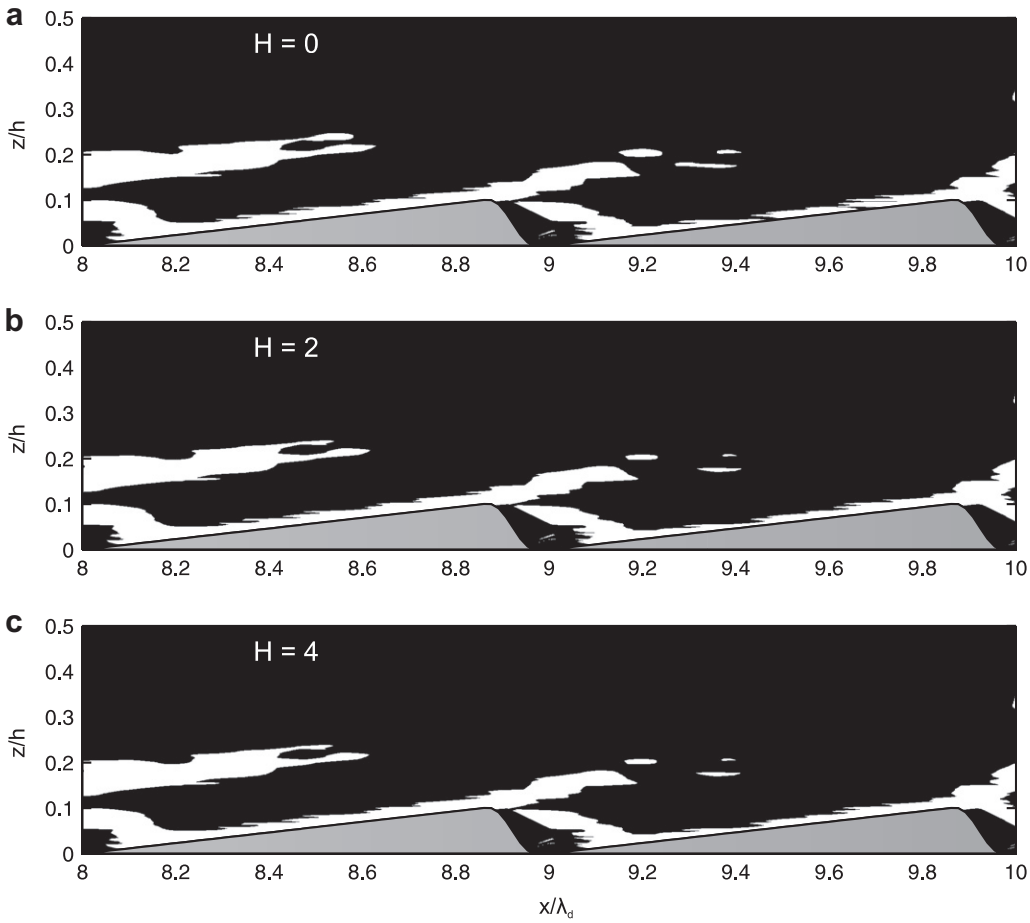

Fig. 13. Spatial distribution of the dominant sweeping events: (a) for threshold parameter $H = 0$, (b) for $H = 2$, (c) for $H = 4$. White region represents the region of sweeping dominance.

dominance is not totally isolated; near the surface ejections are dominant, then sweeps overcome the ejection and again ejection occurs. At the interface of these two regions, the interaction of ejection and sweeps occurs, which may play a key role in the kolk-boils phenomena [24]. It has been observed that some sediment could be ejected from the river bed into suspension due to kolk-boils formation. It seems that inside the pathway of the kolk-boil ejection the fluid pressure is low enough to form a negative pressure gradient and pick up sediment particles into suspension. As a result not only some large scale vortices can be seen on the flow surface, but sediment concentration in these vortices is high and some of the suspended particles are coarse [30]. As the value of threshold parameter H increases the region of sweeping decreases implying the higher shear stresses are generated mainly due to ejection.

4. Discussions

The flow structure generated over asymmetric river dunes has many important implications to the flow resistance, bed shear stress, sediment transport processes and the evolution of alluvial systems. The above considerations motivate the need to investigate the role of 2-D bed form structures to the flow field and sediment transport. For understanding these phenomena previous researchers have focused on only one or two bedform structures (collecting the velocity data in experimental channels). The novelty of the present work is the collection of velocity data over successive fixed asymmetric dunes in an experimental channel and the investigation of the evolution and development of the turbulent flow region over the successive dunes. Thus we greatly expand the spatial scale of the flow region. The results are evaluated in terms of turbulence characteristics. One result is the turbulence shear stress, which increases upwards in the downstream direction. The high magnitude of the shear stress near the dune surface could be responsible for erosion of scour pits over the dunes. Moreover, an 'effective shear stress layer' is observed, which grows from the leading dune up to the seventh dune length ($x/\lambda_d \approx 7.0$) beyond which the entrance effect disappears. The growth of shear stress over the dunes indicates that the flow is not only responsible for transporting sediment as bed load, but it has also more potential to carry the sediment as suspended load. The flow separation at the crest point induces wakes that grow and are transported downstream occupying the outer flow towards the free surface. The wakes incoming from the upstream series of

dunes may be regarded as stacked wakes [29]. As the flow progresses up the dune stoss, the shear stress increases and reaches maximum value at the middle of the separation cell, then again decreases and reaches minimum at the crest which is due to flow acceleration and streamline compression. The flow acceleration reduces the turbulent fluctuations and increases the flow stability as the flow approaches the dune crest.

The ratio of ejection to sweeping events has been computed to find the dominant event throughout the depth. Ejections are responsible for putting sediment into suspension while sweeping causes bedload. Sweeping events dominate within the separation zone, at the reattachment point and at the dune crest (Fig. 13). These turbulent events are responsible for erosion and transport of sediment over the lower stoss side of the dune and deposition on the slip-face of the dune [1].

The near-bottom flow region over the dune covered surface, composed of the separation cell and the internal boundary layer, is influenced by the wakes and the shear layer. These two flow features are important for understanding sediment movement, the stability of bed forms and dune/ripple migration. Large-scale vorticity is manifested as ejection events and arises both along the shear layer and at flow reattachment [1]. These coherent flow structures are advected with the mean flow, often reaching the free surface and erupting as surface 'boils'. The origin of kolks and boils in the fluvial systems has been vigorously attributed to the boundary-layer bursting process [15,4], and may contain higher concentrations of sediment in suspension than the surrounding flow [40]. This flow structure generated over asymmetric river dunes has many important implications to the flow resistance and sediment transport. For instance, the pressure difference over the dune, generated by flow separation and flow acceleration/deceleration associated with the dune form, generate a net force on the dune. In fact, the prediction of sediment transport over dunes, a key aspect of many applications of dune research, relies on being able to estimate the shear stress over the dune and to link this to sediment transport equations.

5. Conclusions

The purpose of this study was to ascertain the influence of bottom roughness on the main flow over a series of 2-D asymmetric dune shaped structures placed successively at the flume surface. A development of turbulent boundary layer thickness along the flow over the dune covered surface is observed, in which the flow characteristics vary up to seventh dune, and beyond which the entrance effect disappears. The study over two selected dunes in the fully developed region reveals the flow separation at the dune crest and the length of separation zone is found to be $5.8H_d$. Streamline compression, flow acceleration and the internal boundary layer structure are clearly visible from the results.

The relative dominance of ejection and sweep events varies along the dunes in an oscillatory pattern at the near bed region, whereas such pattern seems to be disappeared towards the outer flow. Near the bed surface sweeping and ejection events contribute in a cyclic manner (spatially) along the stream-wise direction. At an elevation of 0.4 cm along the dune length sweeping events are found to contribute more to the shear stress generation throughout the dune length. Sweeping and ejections provide an extraction of energy from the complex flow field and these two events are considered to be more important than the interaction events in sediment entrainment. This work elucidates the impact of wavy bed roughness on the main flow, which are responsible for sediment transport process in rivers and estuaries.

Acknowledgement

Authors would like to express their sincere thanks to Prof. R.J. Garde and three anonymous reviewers for valuable comments and suggestions to improve the quality of the paper. The discussions with Prof. S. R. McLean, during his visit to ISI, Calcutta helped a lot in improving the quality of the manuscript. They are also grateful to the Department of Science and Technology (DST), New Delhi for providing the financial support (No. ESS/23/VES/109/2000) for conducting this research.

References

[1] Bennett SJ, Best JL. Mean flow and turbulence structure over fixed, two-dimensional dunes – implications for sediment transport and bedform stability. Sedimentology 1995;42(3):491–513.
[2] Best JL, Kostaschuk RA, Villard PV. Quantitative visualization of flow fields associated with alluvial sand dunes: results from the laboratory and field using ultrasonic and acoustic Doppler anemometry. J Visual 2001;4:373–81.
[3] Best J, Kostaschuk R. An experimental study of turbulent flow over a low-angle dune. J Geophys Res 2002;107(C9):3135. doi:10.1029/2000JC000294.
[4] Best J. Fluid dynamics of river dunes: a review and some future research directions. J Geophys Res 2005;110:F04S02. doi:10.1029/2004JF000218.
[5] Bradshaw P. Analogy between streamline curvature and buoyancy in turbulent shear flow. J Fluid Mech 1969;36:177–91.
[6] Cellino M, Lemmin U. Influence of coherent flow structures on the dynamics of suspended sediment transport in open-channel flow. J Hydr Eng ASCE 2004;130(11):1077–88.
[7] Costello WR, Southard JB. Flume experiments on lower-flow regime bed forms in coarse sand. J Sediment Petrol 1981;51:849–64.
[8] Dalrymple RW, Knight RJ, Lambiase JJ. Bedforms and their hydraulic stability relationships in a tidal environment, Bay of Fundy, Canada. Nature 1978;275:s100–4.
[9] Engel P. Length of flow separation over dunes. J Hydraul Div ASCE 1981;107(HY10):1133–43.
[10] Engelund F, Fredsoe J. Sediment ripples and dunes. Ann Rev Fluid Mech 1982;14:13–37.
[11] Gabel SL. Geometry and kinematics of dunes during steady and unsteady flows in the Calamus River, Nebraska, USA. Sedimentology 1993;40(2):237–69.

[12] Guy HP, Simons DB, Richardson EV. Summary of alluvial channel data from flume experiments, 1956–1961. US Geol Surv Prof Pap 1966;462-I:1–96.
[13] Hurther D, Lemmin U, Blanckaert K. A field study of transport and mixing in a river using an acoustic Doppler velocity profiler. In: Proceedings of river flow, Belgium: Louvain-la-Neuve; 2002.
[14] Ikeda T, Matsuzaki Y. Separable and reattachable flow model for collapsible tube-flow analysis. J Biomech Eng 1999;121: 153–9.
[15] Jackson RG. Sedimentological and fluid dynamic implications of the turbulent bursting phenomenon in geophysical flows. J Fluid Mech 1976;77:531–60.
[16] Julien PY, Klaassen GJ. Sand-dune geometry of large rivers during floods. J Hydraul Eng ASCE 1995;121(9):657–63.
[17] Kostaschuk RA. A field study of turbulence and sediment dynamics over subaqueous dunes with flow separation. Sedimentology 2000;47(3):519–31.
[18] Kostaschuk R, Villard P, Best J. Measuring velocity and shear stress over dunes with acoustic Doppler profiler. J Hydraul Eng ASCE 2004;130:932–6.
[19] Kostaschuk RA, Villard P. Flow and sediment transport over large subaqueous dunes-Fraser river, Canada. Sedimentology 1996;43(5): 849–63.
[20] Lu SS, Willmarth WW. Measurements of the structure of the Reynolds stress in a turbulent boundary layer. J Fluid Mech 1973;60:481–511.
[21] Lyn DA. Turbulence measurements in open channel flows over artificial bedforms. J Hydraul Eng 1993;119:306–26.
[22] Maddux TB, Nelson JM, McLean SR. Turbulent flow over 3D dunes. I: Free surface and flow response. J Geophys Res 2003;108(F1):6009. doi:10.1029/2003JF000017.
[23] Maddux TB, Nelson JM, McLean SR. Turbulent flow over 3D dunes. II: Spatially-averaged stress response. J Geophys Res 2003; 108(F1):6010. doi:10.1029/2003JF000018.
[24] Mao Y. The effects of turbulent burstings on the sediment movement in suspension. Int J Sediment Res 2003;18(2):148–57.
[25] Matthes GM. Macroturbulence in natural stream flow. Trans Am Geophys Union 1947;28:255–65.
[26] Mazumder BS, Ray RN, Dalal DC. Size distribution of suspended particles in open channel flow over sediment beds. Environmetrics 2005;16:149–65.
[27] Mazumder BS, Ojha SP. Turbulence statistics of flow due to wave-current interaction. Flow Meas Instrum 2007;18:129–38.
[28] Nakagawa H, Nezu I. Prediction of the contribution to the Reynolds stress from bursting events in open-channel flows. J Fluid Mech 1977;80(1):99–128.
[29] Nelson JM, Smith JD. Mechanics of flow over ripples and dunes. J Geophys Res 1989;94(C6):8146–62.
[30] Nezu I, Nakagawa H. Turbulence in open channel flow. IAHR monograph series. Rotterdam: A.A. Balkema; 1993.
[31] Nezu I, Rodi W. Open-channel flow measurements with a laser Doppler anemometer. J Hydraul Eng ASCE 1986;112(5):335–55.
[32] Nikora VI, Koll K, McLean SR, Dittrich A, Aberle J. Zero-plane displacement for rough-bed open-channel flows. In: Proceedings of the international conference on fluvial hydraulics, river flow 2002, Belgium: Louvain-la-Neuve; 2002.
[33] Raupach MR. Conditional statistics of Reynolds stress in rough wall and smooth wall turbulent boundary layers. J Fluid Mech 1981;108:363–82.
[34] Richards KJ. The formation of ripples and dunes on an erodible bed. J Fluid Mech 1980;99:597–618.
[35] Robert A, Uhlman W. An experimental study on the ripple dune transition. Earth Surf Process Landforms 2001;26:615–29.
[36] Sengupta S. On trough cross-beddings of fluvial origin. Brahmaputra symposium, Geological survey of India, Misc. Pub. No. 46, 1972. p. 99–107.
[37] Smith JD, McLean SR. Spatially-averaged flow over a wavy surface. J Geophys Res 1977;82:1735–46.
[38] SonTek Inc. ADV principles of operation. San Diego, Calif: 2001. p. 7.
[39] Soulsby R. Dynamics of marine sands, ASCE. Thomas Telford Ltd.; 1997. p. 124.
[40] Venditti JG, Bennett SJ. Spectral analysis of turbulent flow and suspended sediment transport over fixed dunes. J Geophys Res – Oceans 2000;105(C9):22035–47.
[41] Wiberg PL, Nelson JM. Unidirectional flow over asymmetric and symmetric ripples. J Geophys Res 1992;97:12745–61.